SIMPLIFIED METHOD FOR OPTIMAL DESIGN OF FRICTION DAMPER SLIP LOADS BY CONSIDERING NEAR-FIELD AND FAR-FIELD GROUND MOTIONS

(Effect of near and far-field earthquakes on optimum design of friction dampers)

N. Nabid[a], I. Hajirasouliha[b] and M. Petkovski[c]

[a] PhD Candidate, Department of Civil and Structural Engineering, The University of Sheffield, Sheffield, UK.
E-mail: nnabid1@sheffield.ac.uk (Corresponding Author), ORCID ID: 0000-0003-2249-1413

[b] Senior Lecturer, Department of Civil and Structural Engineering, The University of Sheffield, Sheffield, UK.
E-mail: i.hajirasouliha@sheffield.ac.uk, ORCID ID: 0000-0003-2597-8200

[c] Lecturer, Department of Civil and Structural Engineering, The University of Sheffield, Sheffield, UK.
E-mail: m.petkovski@sheffield.ac.uk, ORCID ID:0000-0002-3788-0772

Abstract

A simplified method is proposed for optimum design of friction dampers by considering the characteristics of design earthquakes. Optimum slip loads for 3, 5, 10, 15 and 20-storey RC frames with friction wall-dampers are obtained for a set of 20 near and far-field earthquakes as well as artificial spectrum-compatible records scaled to different acceleration levels. Optimum solutions are shown to be more sensitive to Peak Ground Velocity (PGV) than Peak Ground Acceleration (PGA), especially for near-field earthquakes with high velocity pulses. For identical PGA levels, far-field earthquakes on average result in 1.5 times lower optimum slip loads compared to near-field records, while they lead to 118% higher energy dissipation and 24% lower maximum inter-storey drifts. Empirical equations are proposed to predict optimum slip loads (as a function of number of storeys and PGA/PGV of design earthquakes) and their efficiency is demonstrated through selected examples.

Keywords: Near- and far-field earthquakes; Optimum design; Friction damper; Slip load distribution; Energy dissipation.

1. Introduction

Friction-based passive energy dissipation devices have been successfully used in practice to enhance seismic performance of both newly designed and existing structures subjected to strong earthquake excitations [Vezina and Pall, 2004; Pasquin et al., 2004; Shiraia et al. 2019]. Different types of friction-based dampers have been developed recently including friction wall dampers [Nabid et al. 2017], rotational friction dampers [Mualla and Belev, 2017], friction braced frames [Tirca et al., 2018], and posttensioned concrete walls with friction devices [Guo et al., 2017]. However, finding the optimum values of slip loads in the friction devices (the loads

at which the friction devices start slipping and hence dissipating energy) is challenging, since these values can be sensitive to the characteristics of the seismic excitation.

Several research studies have been carried out on optimum design of friction dampers under earthquake excitations using different optimisation techniques such as Genetic Algorithm (GA) [Moreschi and Singh, 2003; Mohammadi et al., 2018], backtracking search optimisation algorithm (BSA) [Miguel et al., 2016] and Uniform Distribution of Deformation (UDD) [Nabid et al., 2018], or used iterative methods to find the optimum range of slip load values. However, the aforementioned optimisation approaches are computationally expensive and/or require complex mathematical calculations, and therefore, may not be directly used in practical applications. On the other hand, most of the existing research studies on optimum design of friction dampers have been either based on a code-based design spectrum, a set of spectrum-compatible natural/synthetic earthquakes or a single natural earthquake [Petkovski and Waldron, 2003; Pall and Pall, 2004; Lee et al., 2008; Shirkhani et al., 2015; Nabid et al., 2017], where the effects of different types of earthquakes have been neglected. For more accurate design, however, the earthquake uncertainties should be taken into account in terms of fault type, earthquake intensity, peak acceleration and velocity, frequency content, duration, earthquake magnitude and distance.

In an early attempt, a design slip load spectrum was developed by Filiatrault and Cherry [1990] to obtain the best slip load distribution for friction dampers by minimising an energy performance index while considering the properties of the structure and the ground motion anticipated at the construction site. They concluded that the optimum slip load is not only a structural property but also depends on the frequency and amplitude of the ground motion. The values of the optimum slip loads in their study were shown to be linearly proportional to the peak ground acceleration of the input earthquake. In a more recent study, Kiris and Boduroglu [2013] investigated the correlation between the peak displacement demand of a RC structure with friction damper and different parameters used to measure the severity of ground motions. It was demonstrated that depending on the fundamental period of the frame, the strength ratio of the system at slip displacement and the soil profile, different ground motion parameters can play a dominant role in the seismic response of the structure.

Previous studies show that structures designed using older seismic design provisions, based on far-field earthquakes, may experience extensive damage or failure in case of near-field earthquakes [Alavi and Krawinkler, 2001]. The main reason is that large displacement demands can be imposed to the structures by severe pulses of near-field ground motions compared to the far-field earthquakes. In pulse-like ground motions, the amplitude and period of the pulse in the velocity time history are the key parameters to control the performance of the structures, and therefore, they should be taken into account for both design and retrofit of structures in the near-field zones [Alavi and Krawinkler, 2001]. There is also displacement amplification in the long-period structures caused by the large amplitudes in the long period range of displacement response spectra [Anderson and Bertero, 1987]. The results of Alavi ansd Krawinkler [2001] study indicated that conventional retrofit techniques accompanied by increasing the stiffness and/or strength of the system are not efficient for long-period structures subjected to severe pulse-like earthquakes. This is due to moving the structure into a range of higher spectral accelerations by increasing the stiffness (or decreasing the period) of the system. Unlike the cumulative effects of far-field ground motions, the structure dissipates the earthquake input energy in few large displacement excursions under near-field records, where most of the seismic input energy arrives in a

single long-period velocity pulse associated with forward directivity or fling step displacements and response amplification of the long-period structures [Somerville, 1998].

Tirca et al. [2003] investigated the response of middle-rise steel moment-resisting frames with and without shear link (SL) devices subjected to near-field ground motions. Based on their results, the near-field earthquakes expose the structure to higher ductility demands than the far or intermediate-field ground motions. Also, they showed that for the stiffer structures, the shear forces were generally higher at the upper storeys. In a study performed by Xu et al. [2007], the performance of yielding and viscous passive energy dissipation systems were investigated subjected to near-field ground motions by using an analytical ground velocity pulse model. They concluded that the performance of different passive energy dissipation systems depends significantly on the period of the pulse excitation, and therefore, to achieve the best performance, the pulse periods must be taken into account when designing passive energy dissipation systems. Lin et al. [2010] evaluated the efficiency of using initially accelerated passive tuned mass damper (PTMD) to reduce the dynamic responses of structures under near-fault ground motion records. They showed that an appropriate PTMD initial velocity used to accelerate the motion can efficiently reduce the local peak seismic responses of the system under near-fault earthquakes. In another relevant study, Hatzigeorgiou and Pnevmatikos [2014] developed a straightforward method for the evaluation of effective velocities and damping forces for single-degree-of-freedom (SDOF) structures with supplemental viscous dampers under near-source earthquakes. Using their proposed method, it was observed that the inelastic velocity ratio is strongly affected by the period of vibration, the effective viscous damping ratio, the forced reduction factors and the type of seismic fault mechanism. Bhandari et al. [2017] investigated the behaviour of a base-isolated building structure subjected to far-field and near-field earthquakes with directivity and fling-step effects. According to their results, under the near-field earthquakes with fling-step effect, the base isolation proved to be ineffective in terms of reducing base shear, top storey absolute acceleration and maximum inter-storey drift. In a more recent study, Castaldo and Tubaldi (2018) investigated the effects of ground motion characteristics on the optimum friction pendulum properties of seismic isolation systems. It was shown that PGA/PGV is a better indicator of the frequency content of the input ground motion compared to PGA, and can help to provide less scatter predictions.

The research on the effects of near and far-field earthquakes is mainly focussed on the efficiency of base-isolated systems, viscous dampers and semi-active control devices, with few efforts in the design of friction-based passive control systems subjected to the near and far-field records. This study aims to evaluate the effects of near-field and far-field ground motions on optimum design of friction wall dampers leading to a maximum amount of energy dissipation efficiency in friction devices. To achieve this, at first, a comprehensive parametric study is performed on 3, 5, 10, 15 and 20-storey RC frames equipped with friction wall dampers (using a wide range of slip load values) under spectrum compatible earthquakes scaled to different PGA levels as well as a set of 20 near and far-field earthquake records. Based on the results, empirical equations are proposed to obtain the optimum slip load values by considering the effects of number of storeys and earthquake PGA and PGV levels. The efficiency of the proposed design method is then demonstrated through several design examples.

2. Numerical Modelling

To investigate the efficiency of the proposed design methodology, 3, 5, 10, 15, and 20-storey RC frames were designed using the typical geometry shown in Figure 1 (a). The utilised friction damper (schematic view shown in Figure 1 (b)) comprises of a reinforced concrete wall panel connected to the frame system through two vertical supports in the sides, a horizontal connection at the bottom, and a friction device at the top. The connections are designed to avoid transferring extra shear forces to the middle of the adjacent beam and column elements. As shown in Figure 1 (b), the utilised friction device is a conventional Slotted Bolted Connection (SBC) with two steel plates over a central T-shape slotted steel plate anchored to the top floor beam. It should be mentioned that the concrete panels at ground level are fixed to the base to reduce the maximum axial loads in the columns at the ground level. Table 1 lists the period and mass participation factor of the first three modes of vibration for the frames with and without with friction wall-dampers. More detailed information about the adopted friction wall damper can be found in Nabid et al. [2017].

The designed frames were considered to be located in a low-to-medium seismicity region with PGA of 0.2 g and soil type C category of Eurocode 8 [EC8; CEN, 2004a]. The uniformly distributed dead and live loads were considered to be 5.5 kN⁄m^2 and 2.5 kN⁄m^2 for interior floors, and 5.3 kN⁄m^2 and 1.0 kN⁄m^2 for the roof level, respectively. The frames were initially designed based on EC8 [CEN, 2004a] seismic loads and in accordance with the minimum requirements of Eurocode 2 [EC2; CEN, 2004b] for moment-resisting RC frames with medium ductility (DCM). The concrete compressive strength (f_c') and the yield strength of steel reinforcement bars (f_y) were assumed to be 35 MPa and 400 MPa, respectively.

OpenSees software [McKenna and Fenves, 2000] was used to conduct pushover and nonlinear time-history analyses. Concrete sections were modelled using a uniaxial constitutive material with linear tension softening (Concrete02), while the behaviour of steel bars was simulated by a Giuffre–Menegotto–Pinto model (Steel02) with 1% isotropic strain hardening. Beam and column members were divided into three elements and modelled using displacement-based nonlinear beam-column elements with fibre sections while four Gauss–Lobatto integration points were considered for each element. The confinement effects due to the presence of transverse reinforcement were taken into account in the material model of the concrete fibres using *fib* Model Code 2010. P-Delta effects were taken into account in both pushover and nonlinear time-history analyses. A classical Rayleigh damping model proportional to both mass and stiffness matrices (i.e. $C = \alpha M + \beta K$) was adopted and a constant damping ratio of 0.05 was assigned to the first mode and to the modes at which the cumulative mass participation exceeds 95%.

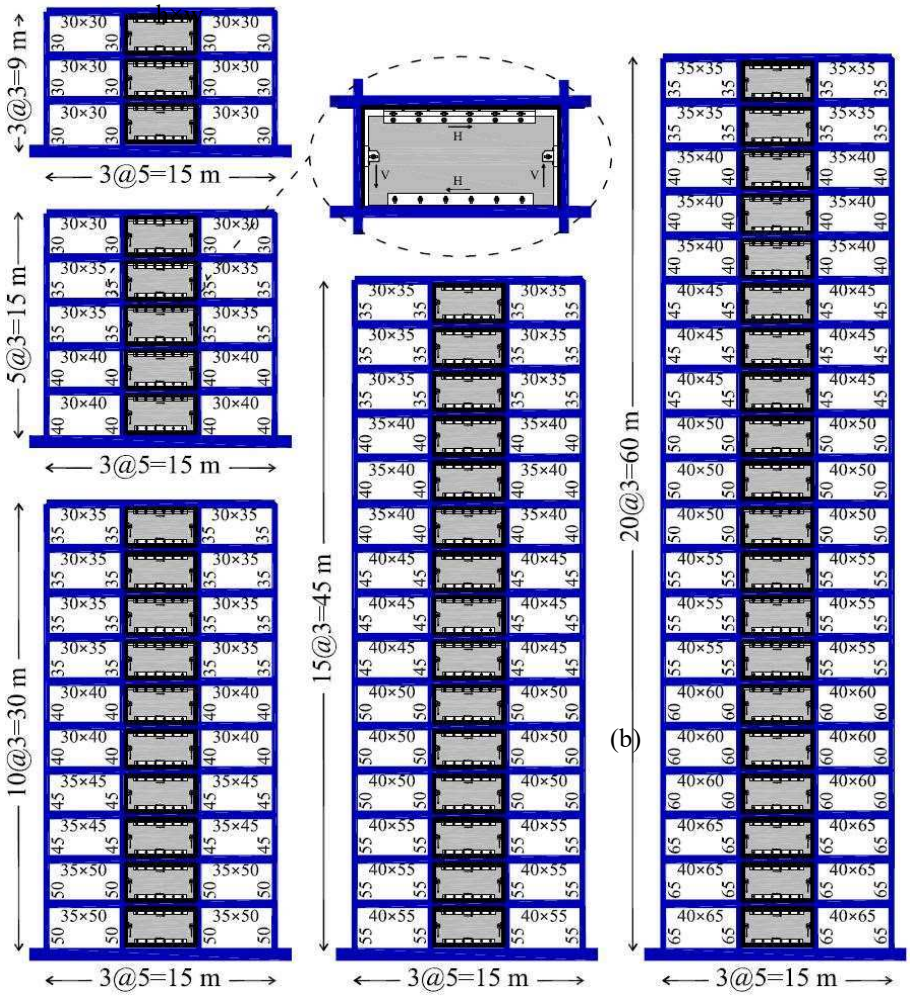

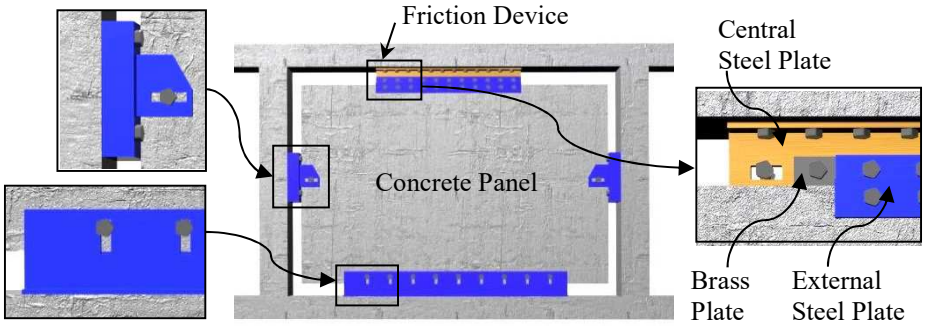

Figure 1. (a) Geometry of the reference RC frames equipped with friction wall dampers, (b) schematic view of the friction wall damper (adopted from Nabid et al. [2017])

The results of the analytical studies showed that the strength of reinforced concrete wall panels with 15 cm thickness is always higher than the maximum loads transferred from the friction device [Nabid, 2018]. Therefore, in this study the wall panels were modelled using equivalent elastic elements. An inelastic link element, representing an ideal Coulomb friction hysteretic behaviour, was utilised to model the friction device. The beam-to-column connections were assumed to be fully rigid with no shear failure in the panel zones. A computer code in MATLAB [2014] was also developed and linked to the OpenSees [McKenna et al., 2000]

149 software to calculate the energy dissipation in the structural elements and friction devices under earthquake
150 excitations.

151 **Table 1.** Period and mass participation factor of the first three modes of vibration

		Frames without friction dampers		Frames with friction dampers	
		Fundamental Period (sec)	Mass Participation Factor	Fundamental Period (sec)	Mass Participation Factor
3- Storey	Mode 1	0.71	82.9%	0.15	81.9 %
	Mode 2	0.22	14.1%	0.06	10.4 %
	Mode 3	0.12	2.8%	0.04	6.7 %
5- Storey	Mode 1	0.99	77.7%	0.29	73.8 %
	Mode 2	0.32	11.8%	0.08	15.7 %
	Mode 3	0.17	5.7%	0.05	5.7 %
10- Storey	Mode 1	1.56	78.1%	0.78	68.3 %
	Mode 2	0.55	10.0%	0.19	18.1 %
	Mode 3	0.31	4.3%	0.09	6.4 %
15- Storey	Mode 1	1.93	75.0%	1.29	65.1 %
	Mode 2	0.73	11.5%	0.33	17.3 %
	Mode 3	0.42	4.7%	0.15	6.1 %
20- Storey	Mode 1	2.31	73.1%	1.78	64.3 %
	Mode 2	0.84	11.1%	0.47	16.2 %
	Mode 3	0.49	4.0%	0.22	5.9 %

152

153 3. Characteristics of Near-field Earthquakes

154 In general, the distance of the structure from the fault rupture is one of the dominant factors influencing the
155 imposed peak displacement demand. The near-field zones are typically considered to be within 12 km from the
156 fault rupture, while far-field regions are those with epicentral distances of the recording stations ranging from 12
157 to 64 km [Chopra and Chintanapakdee, 2001]. Some researchers have classified near-field zones as those within
158 20-60 km from the fault rupture [Stewart et al., 2002]. In general, in a near-field zone and at a particular site, the
159 earthquake characteristics are significantly influenced by three factors: the rupture mechanism, slip direction
160 relative to the site and the residual ground displacement at the site due to the tectonic movement. Forward-
161 directivity pulses usually occur when the rupture propagation velocity is close to the shear-wave velocity and
162 the direction of slip on the fault is aligned with the site (mainly oriented in the fault-normal direction due to the
163 radiation pattern of the fault) [Somerville and Smith, 1996; Bray and Rodriguez-Marek, 2004; Davoodi and
164 Sadjadi, 2015]. Due to forward-directivity effect, large-amplitude pulses of motion are generated with long
165 period (1–1.5 s) and short duration while having a high ratio of Peak Ground Velocity (PGV) to Peak Ground
166 Acceleration (PGA) [Somerville et al., 1997]. Therefore, in near-field areas high velocity pulses, which are
167 extremely destructive in nature, are one of the main factors to define the severity of the seismic input rather than
168 the PGA value. Regarding the last factor, the tectonic deformation associated with the fault rupture may contain
169 a significant permanent static displacement termed fling-step effect [Bray and Rodriguez-Marek, 2004]. It
170 produces a high amplitude velocity pulse and a monotonic step in the displacement time history [Somerville,
171 2002]. Additionally, hanging wall and footwall effects can be observed in dipping fault earthquakes. The fault

plane has generally closer proximity to the sites on the hanging wall than the sites on the footwall at the same distance. The hanging wall sites have larger amplitude and slower attenuation in ground motion parameters than the footwall sites with the same distance. These effects have higher influence on the acceleration spectra in short periods. The aforementioned fling-step effect is the relative slip between the hanging wall and footwall [Abrahamson and Somerville, 1996].

Near-field earthquakes transfer a major portion of fault energy in the form of pulses, which can be frequently seen in displacement, velocity, and acceleration time histories. These pulses tend to have high Fourier spectrum in limited periods, while in far-field earthquakes the high Fourier spectrum generally occurs in broad range of periods [Iwan, 1994; Bhandari et al., 2017]. In the frequency domain, depending on the fault-normal or fault-parallel components of the forward-directivity ground motions in near-field region, near-field earthquakes can have either higher or lower frequency contents compared to the far-field earthquakes [Davoodi and Sadjadi, 2015]. Davoodi and Sadjadi [2015] also showed that the maximum Fourier amplitudes of far-field earthquakes and fault-parallel component of forward-directivity ground motions are distributed at higher frequencies (mostly beyond 1Hz) compared to the maximum Fourier amplitudes of near-field earthquakes with fling-step and fault-normal component of forward-directivity records which generally occurs at frequencies less than 1Hz. It was demonstrated by Malhotra [1999] that, for the same PGA and duration of shaking, ground motions containing directivity pulses can result in much higher base shear, inter-storey drift, and roof displacement in high-rise structures as compared to those without pulses.

4. Ground Motion Datasets

4.1. Natural Near-field and Far-field Earthquake Records

In this study, two sets of 10 near-field and 10 far-field ground motions were used to evaluate the seismic performance of the 3, 5, 10, 15 and 20-storey frame structures with friction wall dampers. All the selected ground motions correspond to soil class C of EC8 with surface magnitudes ranging from 6.5 to 7.4. Tables 2 and 3 list the designations and characteristics of the selected unscaled near-field and far-field ground motions, respectively. The rupture distances (R: distance from the fault rupture plane to the site) are within 10 km for the near-field records and between 12 and 30 km for the selected far-field ground motions. The fault rupture mechanisms are strike slip and reverse for all the records. It should be noted that the forward directivity effect of the near-field ground motions generally leads to more intense fault-normal component compared to the fault-parallel component [Somerville, 1998]. In this study, the fault-normal components with higher intensities were selected for the nonlinear time history analyses.

Figures 2 (a) and (b) compare the 5% damped elastic acceleration and velocity response spectra of the studied unscaled near-field and far-field earthquakes, respectively. The acceleration response spectra show that the mean spectrum of the near-field earthquakes is well above whereas the far-field mean spectrum is well below the EC8 design spectrum. This implies that, with the same range of surface magnitudes, the intensity of near-field records is much higher than those recorded far away from the earthquake epicentre. Although the elastic acceleration response spectrum provides the basis to identify the characteristics of the design earthquakes, in case of near-field ground motions, the acceleration response spectrum does not adequately characterise the

209 design earthquake. This is because near-field earthquakes are mainly characterised by a relatively long period
210 pulse of strong motion with fairly short duration, while the far-field motions have relatively long duration
211 [Somerville, 1998]. Therefore, to better show the characteristics of the selected earthquakes, the elastic velocity
212 response spectra of the selected near-field and far-field earthquakes with their mean spectra are also shown in
213 Figure 2.

214 **Table 2.** Properties of the selected near-field ground motions

No.	Earthquake	Ms	Station	Abr.	R (km)	PGA (g)	PGV (cm/s)	PGV/PGA (s)
1	1999 Duzce	7.14	Duzce	DUZ	6.58	0.515	84	0.166
2	1992 Erzincan	6.69	Erzincan	ERZ	4.38	0.387	107	0.282
3	1994 Northridge	6.69	Rinaldi Receiving Sta	RIN	6.50	0.874	148	0.173
4	1994 Northridge	6.69	Newhall - Fire Sta	NEW	5.92	0.590	97	0.168
5	1994 Northridge	6.69	LA - Sepulveda VA Hospital	SEP	8.44	0.932	76	0.083
6	1995 Kobe	6.9	KJMA	JMA	0.96	0.630	76	0.123
7	1995 Kobe	6.9	Takatori	TAK	1.47	0.671	123	0.187
8	1995 Kobe	6.9	Port Island	POR	3.31	0.290	51	0.179
9	1979 Imperial Valley	6.53	Meloland Geot. Array	MEL	0.07	0.298	93	0.168
10	1979 Imperial Valley	6.53	El Centro Array #4	ARR4	7.05	0.484	40	0.084

215

216 **Table 3.** Properties of the selected far-field ground motions

No.	Earthquake	Ms	Station	Abr.	R (km)	PGA (g)	PGV (cm/s)	PGV/PGA (s)
1	1994 Northridge	6.69	Canoga Park-Topanga Can	CAN	14.70	0.358	34	0.097
2	1994 Northridge	6.69	Northridge-Saticoy St	SAT	12.09	0.459	60	0.133
3	1994 Northridge	6.93	Capitola	CAPIT	15.23	0.511	38	0.076
4	1989 Loma Prieta	6.93	Sunnyvale-Colton Ave.	SUN	24.23	0.207	37	0.182
5	1989 Loma Prieta	6.93	Gilroy Array #3	GIL3	12.82	0.559	36	0.066
6	1987 Superstition Hills	6.54	El Centro Imp. Co. Cent	COC	18.20	0.357	48	0.137
7	1987 Superstition Hills	6.54	Westmorland Fire Station	WES	13.03	0.211	32	0.155
8	1971 San Fernado	6.61	LA - Hollywood Stor Lot	HOLL	22.77	0.225	22	0.100
9	1992 Landers	7.28	Desert Hot Springs	LAN	21.78	0.171	19	0.113
10	1978 Tabas	7.35	Boshrooyeh	TAB	28.79	0.106	13	0.125

217

218

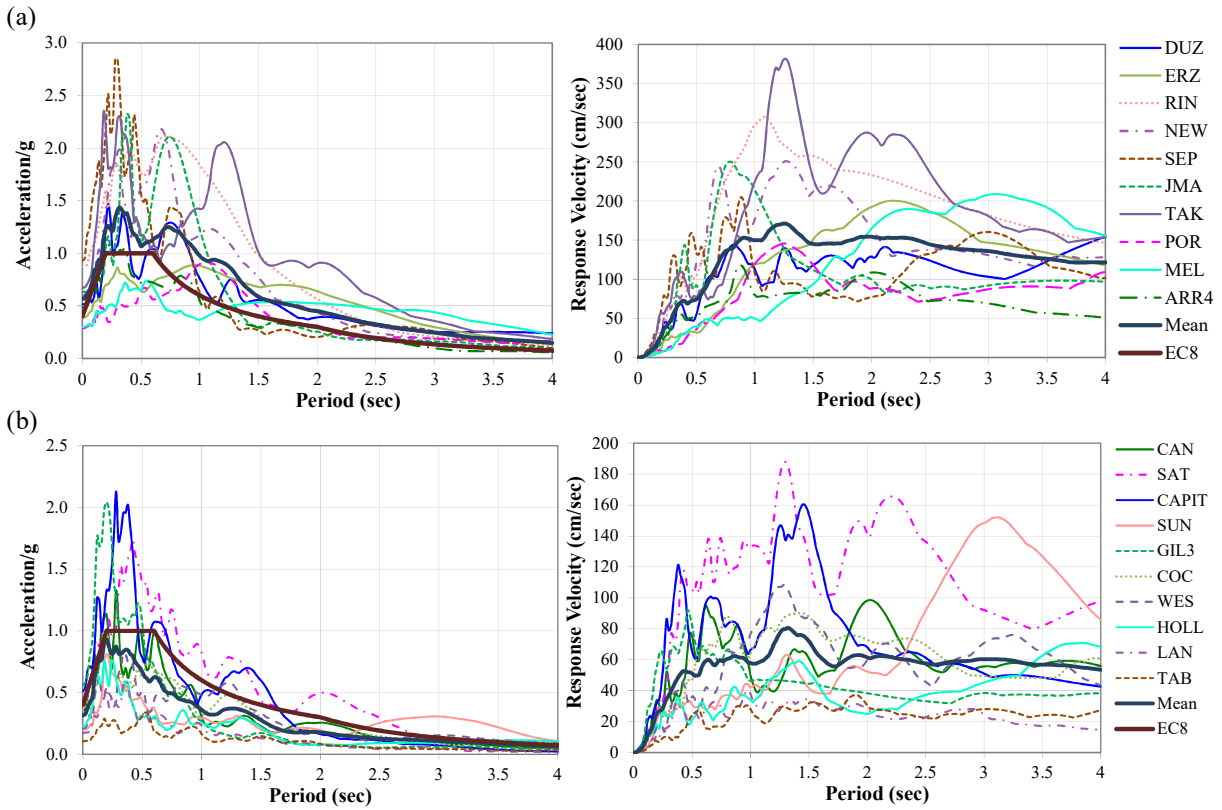

Figure 2. Elastic acceleration and velocity response spectra of the selected (a) near-field and (b) far-field earthquakes and the EC8 design spectrum, 5% damping ratio

Figures 2(a) and (b) show that while the near-field ground motions have a narrower velocity-sensitive region at longer periods, they have wider acceleration-sensitive region compared to the far-field excitation records (except SUN). These results are in agreement with those obtained from the research carried out by Chopra and Chintanapakdee [2001] and Hall et al. [1995]. Figure 3 compares the mean acceleration and velocity response spectra of the selected near and far-field ground motions showing significantly higher values for the near-field records.

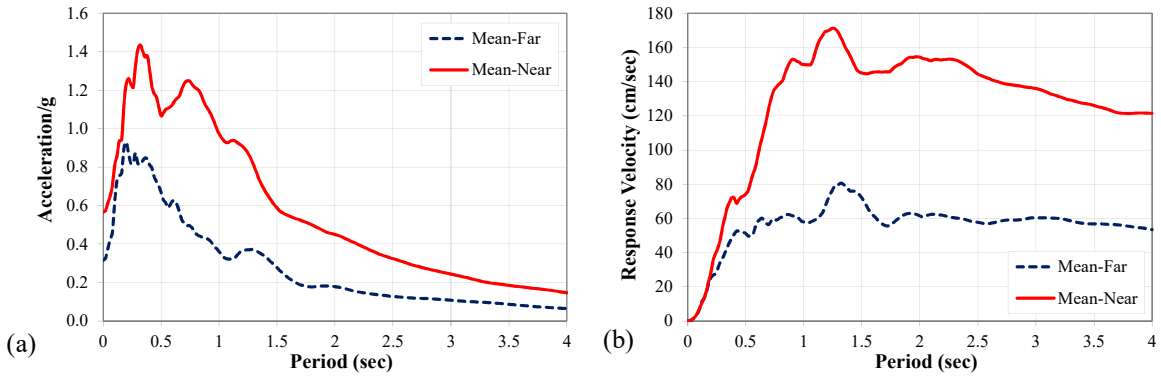

Figure 3. Mean (a) acceleration and (b) velocity response spectra of the selected near-field and far-field earthquakes, 5% damping ratio

4.2. Synthetic Earthquake Record

The previous research by Nabid et al. [2017, 2018] implied that the earthquake uncertainty, in terms of acceleration response spectra, can be efficiently managed by using synthetic earthquakes representing the

average spectrum of a selected set of natural earthquakes. Therefore, a synthetic earthquake is generated using the TARSCTHS [Papageorgiou et al., 2002] program to be compatible with EC8 design response spectrum for high seismicity regions (i.e. PGA=0.4g) and soil class C. Figure 4 shows the good agreement between the elastic acceleration response spectrum of the simulated earthquake record and the corresponding EC8 design spectrum.

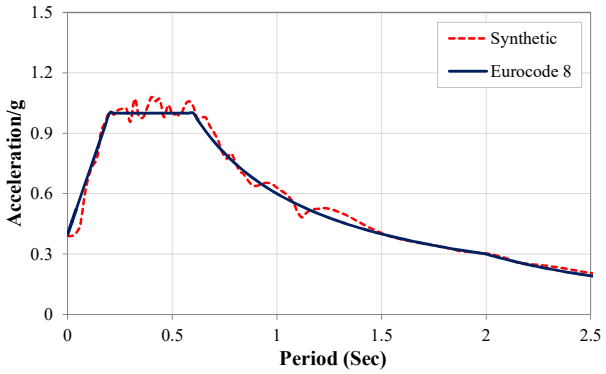

Figure 4. Elastic acceleration response spectra of the synthetic earthquake record and the EC8 design spectrum, 5% damping ratio

5. Effect of Earthquake Intensity Level on Energy Dissipation Efficiency

The synthetic earthquake (compatible with the EC8 spectrum) was utilised to investigate the effect of the peak ground acceleration (PGA) on the maximum energy dissipation efficiency of the selected frames with friction wall dampers. It should be noted that different ground motion parameters may play role in peak structural response demand depending on the system properties and the soil profile (Kiris and Boduroglu, 2013). However, PGA is one of the widely accepted intensity measure parameters that can generally show the pattern of the observed intensities (Wald et al., 1999). The energy dissipation parameter, RW, which is the ratio between the work of the friction devices to the work of the beam and column elements (introduced in [Nabid et al., 2017]), is considered as an effective factor for assessing the efficiency of the proposed friction wall dampers. Figure 5 shows the relationships between the slip load ratio (ratio between the average of slip loads and the average of storey shear strengths at all storey levels) and the energy dissipation parameter, RW, for the 3, 5, 10, 15 and 20-storey frames, subjected to the selected synthetic earthquake with a range of different PGA values (ranging from 0.1g to 1.2g). The optimum value of the slip load ratio is considered to be the one at which the RW factor reaches its peak. The results in Figure 5 show that for stronger earthquakes (higher PGA levels) the optimum slip load ratios are higher and distributed over a wider range. It is also shown that the energy dissipation efficiency (RW) is generally increased for lower earthquake intensity levels. This can be attributed to the fact that most structural elements remain in the elastic (or near elastic) range under low intensity earthquakes. The results also show a clear difference between the optimum ranges of slip load values for structures with different number of storeys as will be taken into consideration in the empirical equations proposed in the following sections.

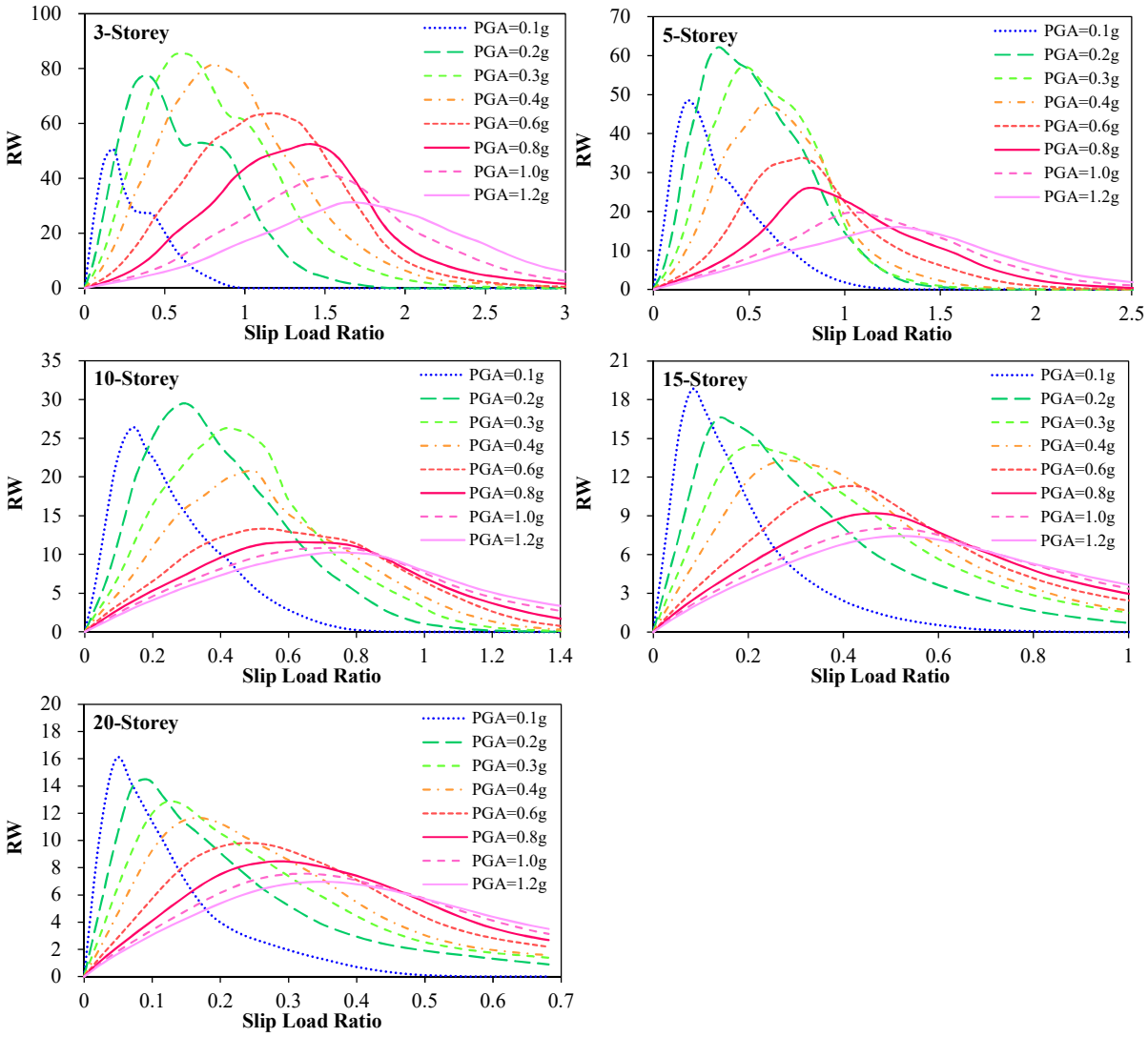

Figure 5. Variation of energy dissipation parameter, RW, of the 3, 5, 10, 15 and 20-storey frames as function of slip load ratio under a synthetic earthquake record with different PGA levels

The results of a previous study [Pall and Pall , 2004] suggested that variations up to ±20% of the optimum slip load do not significantly affect the response; however, the range of these variations depend on the earthquake intensity. The results in Figure 5 imply that this is true for high PGA levels but not for low PGA levels, where the optimum response is significantly affected by small variations in the optimum slip load ratio. The energy dissipation effectiveness of the friction wall dampers in low to medium-rise structures initially increases with the increase of earthquake intensity up to a certain level. For the high-rise structures (15 and 20-storey); however, RW decreases monotonically by increasing the PGA. This can be mainly caused by the high stiffness of the low-rise building that in turn leads to smaller deformation demands under low PGA level earthquakes, and therefore, less energy dissipation through the work of the friction devices. This is more highlighted for the 3-storey frames with almost 70% higher RW for the 0.3g input compared with that for 0.1g. Figure 6 illustrates the variation of the energy dissipated through the work of the friction devices in the 3, 5, 10, 15 and 20-storey frames under the selected synthetic spectrum compatible earthquake with different PGAs. As can be observed, a

negligible amount of energy is dissipated by the friction dampers in the 3 and 5-storey frames under the 0.1g earthquake compared to the other earthquake PGA levels.

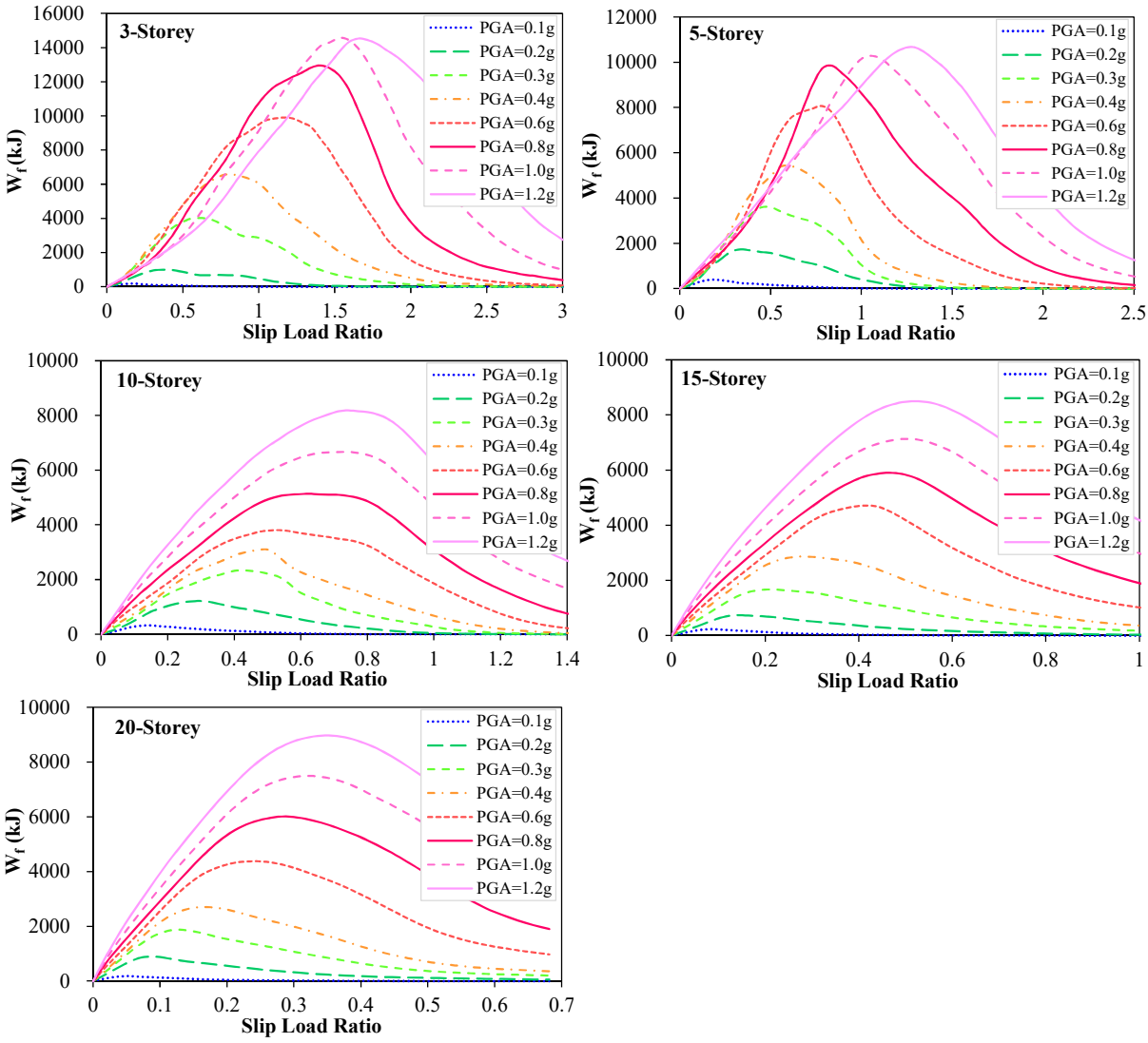

Figure 6. Variation of work of the friction devices for the 3, 5, 10, 15 and 20-storey frames as function of slip load ratio under a synthetic earthquake record with different PGA levels

In this study, the slip load ratios for which the energy dissipation parameter, RW, is greater than 90% of the its maximum value (i.e. less than 10% reduction), are considered as the optimum practical design range. The median (middle point) of the optimum slip load ratio ranges for the selected frames is then calculated under the synthetic spectrum-compatible earthquake using different PGA levels. Based on regression analysis using the median points, the following equation is suggested to calculate the optimum slip load ratio as a function of the earthquake PGA and number of storeys:

$$R_{Syn} = (1.16 \times e^{-0.09n} \times (a_g)^{0.75}) / 100 \quad (1)$$

where R_{Syn} is the optimum slip load ratio obtained for the selected spectrum-compatible synthetic earthquake (see Figure 4) and defined as the ratio between the average of slip loads and the average of storey shear strengths at all storey levels; n is the number of storeys and a_g is the PGA of the design earthquake in cm/s^2. It should be mentioned that, to avoid using very small constant coefficients, the proposed equation is divided by a 100 term. The proposed equation, on average, leads to relatively small errors (9.8%) compared to the results obtained from the parametric study on 3, 5, 10, 15 and 20-storey frames with friction wall dampers. Figure 7 shows the slip load design curves obtained from equation 1 and the corresponding optimum slip load ranges as a function of earthquake intensity (PGA). While Filiatrault and Cherry [1990] suggested that the value of the optimum slip load is linearly proportional to the PGA level, the results of this study show a non-linear relationship between the PGA and optimum slip load values.

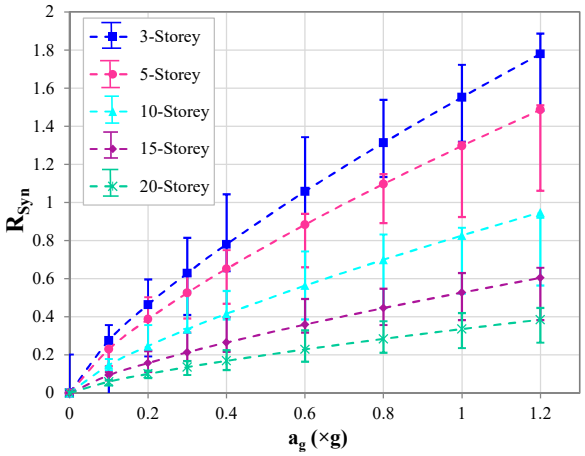

Figure 7. Design slip load ratios for 3, 5, 10, 15 and 20-storey frames as a function of earthquake PGA

While PGA is the parameter most commonly used to identify earthquake intensity, it has also been reported that it is not a totally reliable parameter to assess the seismic performance of structures. For instance, according to Housner and Jennings [1982], peak ground velocity (PGV) can be a better parameter due to its direct connection to energy demand. On the other hand, near-fault impulsive ground motions are often characterised by PGV [Malhotra, 1999; Bray and Rodriguez-Marek, 2004]. For this reason, in the following sections the effect of near-field and far-field earthquake ground motions with variable ranges of both PGA and PGV is investigated in the optimum design of friction dampers.

6. Effect of Near-Field and Far-Field Earthquakes on Optimum Design of Friction Dampers

To evaluate the effect of near-field and far-field ground motions on optimum design solutions, the 3, 5, 10, 15 and 20-storey frames with friction wall dampers are subjected to the natural records listed in Tables 2 and 3. Figures 8 (a) and 8 (b) present the energy dissipation parameter RW, as a function of slip load ratio for the frames under the selected near-field and far-field earthquakes, respectively.

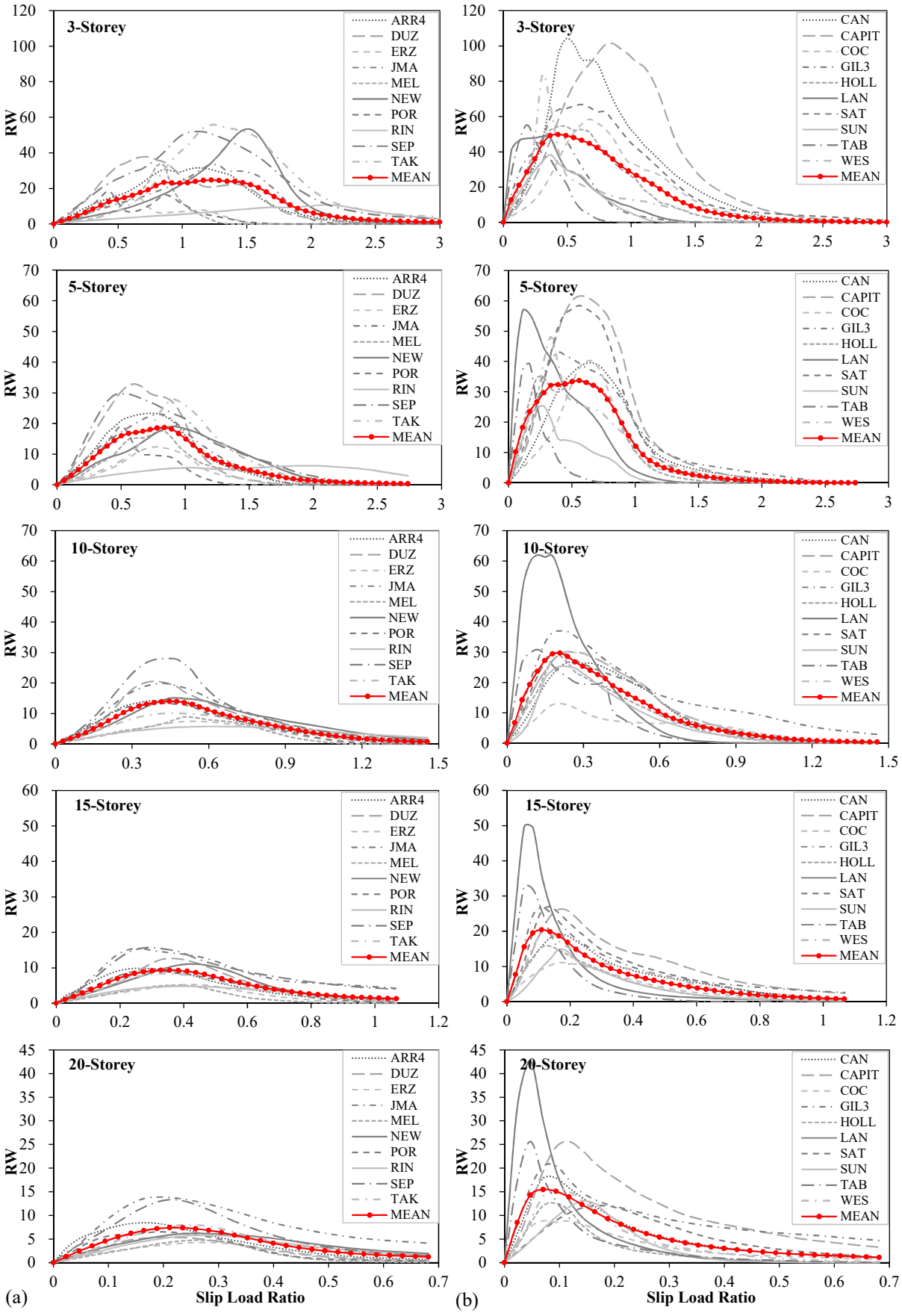

Figure 8. Variation of energy dissipation parameter, RW, of the 3, 5, 10, 15 and 20-storey frames as function of slip load ratio under (a) near-field and (b) far-field ground motions

The comparison of peaks of the mean-value curves shows about twice higher energy dissipation efficiency of the friction dampers for far-field earthquakes (i.e. 2.02, 1.81, 2.13, 2.18 and 2.09 for the 3, 5, 10, 15 and 20-storey frames, respectively). By considering the acceleration and velocity response spectra of the earthquakes (see Figure 2), those records with more intense velocity pulse and/or higher response acceleration (such as SEP, TAK, RIN and JMA from the near-field set, and CAPIT, SAT and GIL3 from the far-field set of earthquakes), in general, result in maximum energy dissipation efficiency at higher slip load ratios. The earthquakes with relatively high velocities at longer periods (e.g. MEL and SUN) led to higher optimum ranges of slip load ratios for taller buildings, compared to their corresponding mean curves; whereas for the low to medium-rise structures their optimum ranges are close to those of the mean curves. On the contrary, for the low to medium-rise frames, the earthquakes with the maximum velocity at lower periods (e.g. RIN) resulted in very high optimum slip load ratios. This is due to the earthquake high velocity occurring at the periods close to the natural period of the structure, and therefore, due to dynamic magnification effects, higher friction forces are required for optimum performance of the structure.

By considering no more than 10% reduction in the maximum of the mean RW curves, the range of optimum slip load ratios for the selected near-field earthquakes can be defined as 0.89-1.51, 0.56-0.95, 0.34-0.54, 0.25-0.44 and 0.17-0.28 for the 3, 5, 10, 15 and 20-storey frames, respectively. The corresponding optimum slip load ratio ranges obtained for the far-field earthquakes are 0.31-0.67, 0.33-0.73, 0.16-0.27, 0.09-0.16 and 0.06-0.12. The results indicate that the near-field earthquakes with higher velocity levels generally lead to higher and wider optimum ranges of slip load ratios for the supplemental friction-based energy dissipation devices compared to the far-field ground motions.

Figure 9 shows the variation of maximum inter-storey drift ratio of the 3, 5, 10, 15 and 20-storey frames as function of slip load ratio under the selected near-field and far-field earthquakes. It should be noted that, for better comparison, the results in Figure 9 are scaled to the maximum inter-storey drifts of the corresponding bare frames. It is shown that the optimum slip load ratio ranges, defined earlier as those leading to the maximum energy dissipation efficiency, also result in minimum drift ratios. The maximum inter-storey drift ratios were, on average, attenuated by 94%, 80%, 55%, 44% and 34% for the 3, 5, 10, 15 and 20-storey frames under the near-field earthquakes, respectively; and by 92%, 85%, 63%, 54% and 42% for the 3, 5, 10, 15 and 20-storey frames under the far-field earthquakes, respectively. In general, the reduction in drift ratios was more noticeable in far-field earthquakes, with the difference between near and far-field increasing with the increase in height of the buildings (i.e. by maximum 24% reduction in 20-storey frame).

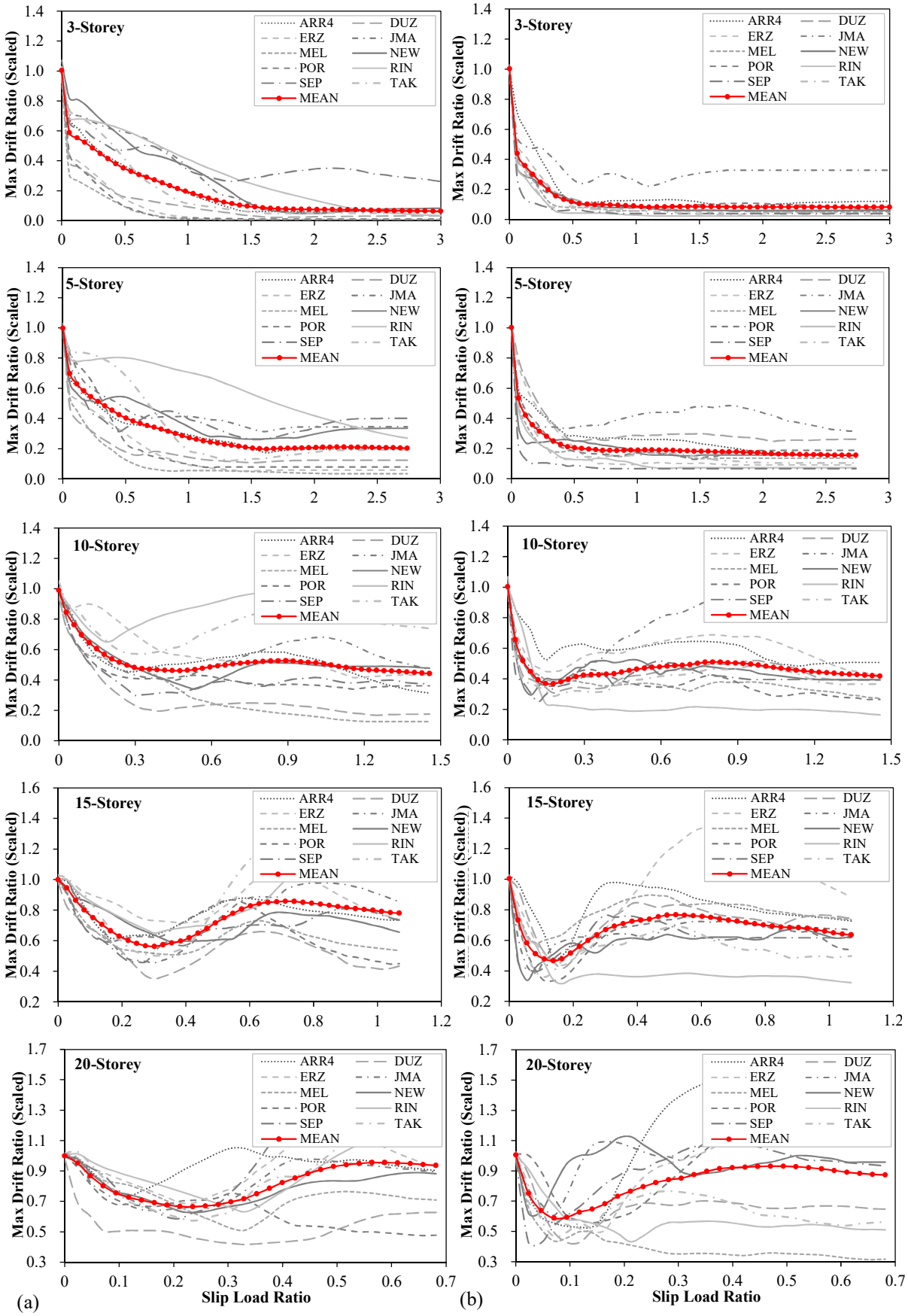

Figure 9. Variation of maximum inter-storey drift ratio (scaled to the bare frame) of the 3, 5, 10, 15 and 20-storey frames as function of slip load ratio under (a) near-field and (b) far-field ground motions

Using individual optimum slip load ratios corresponding to the maximum energy dissipation efficiency obtained for each near-field and far-field earthquake with specific PGA, Equation 1 can be modified to the following equations:

$$R_{near} = (1.29 \times e^{-0.09n} \times (a_g)^{0.75}) / 100 \quad (2)$$

$$R_{far} = (0.86 \times e^{-0.09n} \times (a_g)^{0.75}) / 100 \quad (3)$$

where R_{near} and R_{far} are the optimum slip load ratios estimated for near-field and far-field earthquakes, respectively. Figure 10 shows the variation of optimum slip load ratios of the 3, 5, 10, 15 and 20-storey frames as function of earthquake PGA for the near and far-field earthquakes overlaid with their corresponding design curves (Equations 2 and 3). Equations 2 and 3 are proposed to have, on average, minimum errors (i.e. 27% and 23%) to the optimum results obtained for the near and far-field earthquakes, respectively.

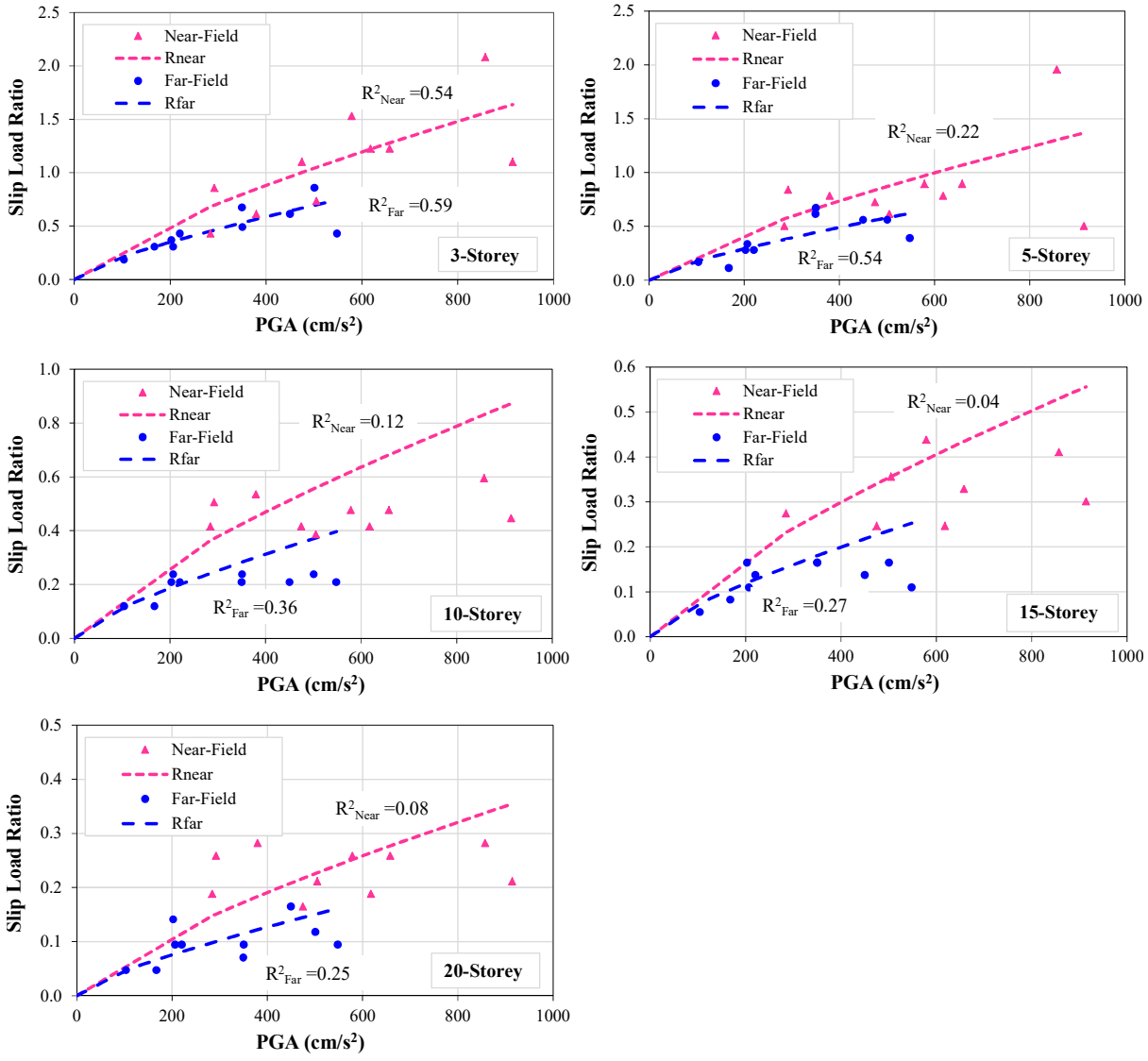

Figure 10. Variation of optimum slip load ratio of the 3, 5, 10, 15 and 20-storey frames as function of earthquake PGA level for the near-field and far-field earthquakes with their corresponding design equation curves (Eq. 2 and 3)

For better comparison, the R-squared values are also calculated for Equations 2 and 3 using the results of the near-field and far-field earthquake records as shown in Fig. 10. It can be seen that in general the proposed equations could not accurately explain the variability of the slip load ratio data as a function of PGA. Especially there are high dispersions of the results (i.e. very low R-squared values) around the proposed equations for the high-rise frames under near-field earthquakes.

Based on Equations 2 and 3, for the same earthquake PGA, on average, near-field earthquakes result in 1.5 times higher optimum slip loads than those for far-field earthquakes. The reason for this is the higher PGV levels of the near-field earthquakes compared to the far-field records. For example, DUZ from the near-field set of earthquake versus GIL3 from the far-field (Table 2) have PGAs of 0.515g and 0.559g, and PGV of 84m/s and 36m/s, respectively. As outlined in Zhu et al. [1988] and Pavel and Lungu [2013], the PGV/PGA ratio can be used as an indicator of both frequency content of strong ground motions and potential structural damage. They revealed that low PGV/PGA ratios generally correspond to ground motions with a high frequency content in the strong-motion phase (e.g. SEP, CAPIT and GIL3), whereas high PGV/PGA ratios, in general, are associated with the ground motions with intense, long-duration acceleration pulses (e.g. TAK and NEW). In pulse-like ground motions, the coherent long-period pulses may lead to the PGV/PGA ratio of ground motions become larger (e.g. ERZ and TAK). Therefore, the ground motions with higher PGV/PGA values generally have larger damage potential [Meskouris at al., 1992]. Ground motions at moderate distances from the energy source normally have a broad range of significant frequency content, resulting in intermediate PGV/PGA ratios (e.g. TAB and LAN).

Figure 11 shows the optimum slip load ratios of the 3, 5, 10, 15 and 20-storey frames under the selected near and far-field earthquakes as function of the earthquake PGV/PGA ratios. For similar PGV/PGA ratios, the earthquakes with higher values of PGA and PGV result in higher optimum slip load ratios (e.g. RIN compared to NEW, DUZ, POR and TAK). Consequently, the earthquake response velocity can be used as a parameter that defines the optimum solution. The following equation calculates the optimum slip load ratios for all types of earthquakes, giving an average error of 18% (better than both Equations 2 and 3) when compared with the results obtained for near and far-field natural earthquakes. This implies that the PGV factor can be a better parameter to estimate the optimum slip load values.

$$R_{EQ} = (4.75 \times e^{-0.09n} \times (a_v)^{0.75}) / 100 \tag{4}$$

where R_{EQ} is the optimum slip load ratio for both near-field and far- field earthquakes and a_v is the PGV of the earthquake.

Finally, by using a previously defined uniform cumulative pattern [Nabid et al., 2017] for the height-wise distribution of slip loads, the equation below can be used to find the slip load values at each storey level:

$$F_{s,i} = \frac{\sum_{1}^{n} F_{y,i} \times 4.75 \times e^{-0.09n} \times (a_v)^{0.75}}{100 \times n(n+1)/2} \times (n+1-i) \tag{5}$$

where $F_{s,i}$ and $F_{y,i}$ are the slip load and the storey shear strength of the i^{th} storey, respectively. It should be noted that the storey shear strength values can be calculated based on the results of non-linear pushover analysis. To avoid the effects of lateral load patterns, to obtain the shear strength of each storey, a single lateral load was applied at the same level, while the lateral degrees of freedom for all lower level storeys were constrained (Hajirasouliha and Doostan, 2010). The load-displacement curves were idealised by using bi-linear model proposed by ASCE/SEI 41-17, where the storey yield displacement is determined on the condition that the secant slope intersects the actual envelope curve at 60% of the nominal storey shear strength while the area enclosed by the bilinear curve up to failure point (here 4% drift) is equal to that enclosed by the original curve.

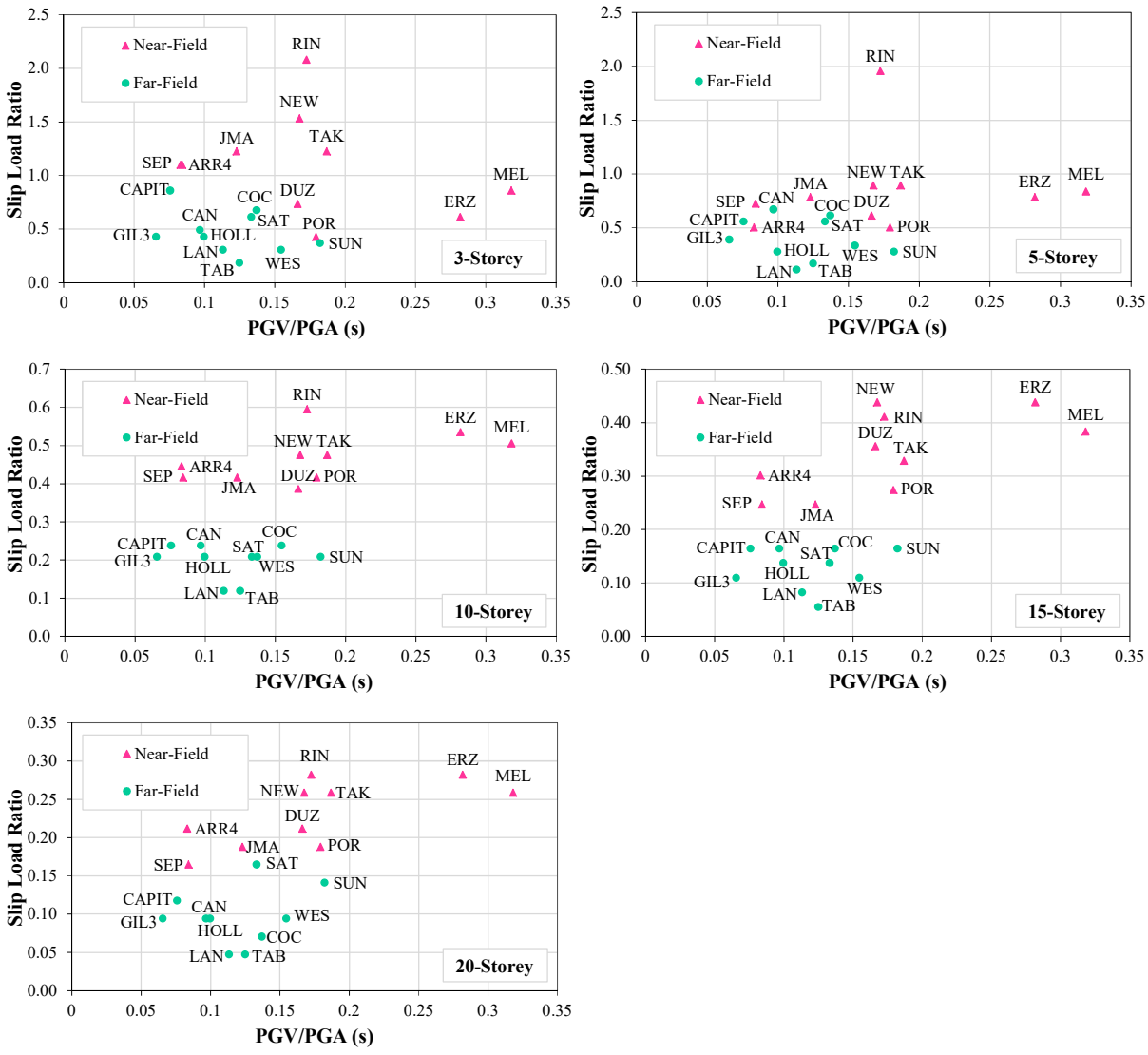

Figure 11. Comparison of optimum slip load ratios of the 3, 5, 10, 15 and 20-storey frames under the selected near and far-field earthquakes as function of earthquake PGV/PGA ratio

The accuracy of the proposed empirical equation (Equation 4) can be assessed from Figure 12, showing the individual optimum slip load ratios obtained for the selected natural near-field and far-field earthquakes and the curves resulting from Equation 4 (as functions of earthquake PGV level). The proposed equation curve is the best fit to the series of optimum slip load ratios obtained for the selected earthquakes. The comparison with the results obtained with Equations 2 and 3, where PGA is the optimisation parameter (Figure 10), shows that PGV

is a more reliable parameter to determine the optimum design solutions for the frames subjected to both near and far-field earthquakes. For all the selected frames, the R-squared values corresponding to Equation 4 are significantly higher than those calculated for Equations 2 and 3, which confirms the higher accuracy of the new equation to predict the optimum slip load ratio under both near and far-field earthquakes.

It can be observed from Figure 12 that the upper parts of the data sets with higher optimum slip load ratios are associated with the results of the near-field earthquakes, whereas the lower parts correspond to those of the far-field records. The dispersion of the results and discrepancy between the data sets and the proposed equation curve can be caused by different pulse periods and frequency contents of the design earthquakes.

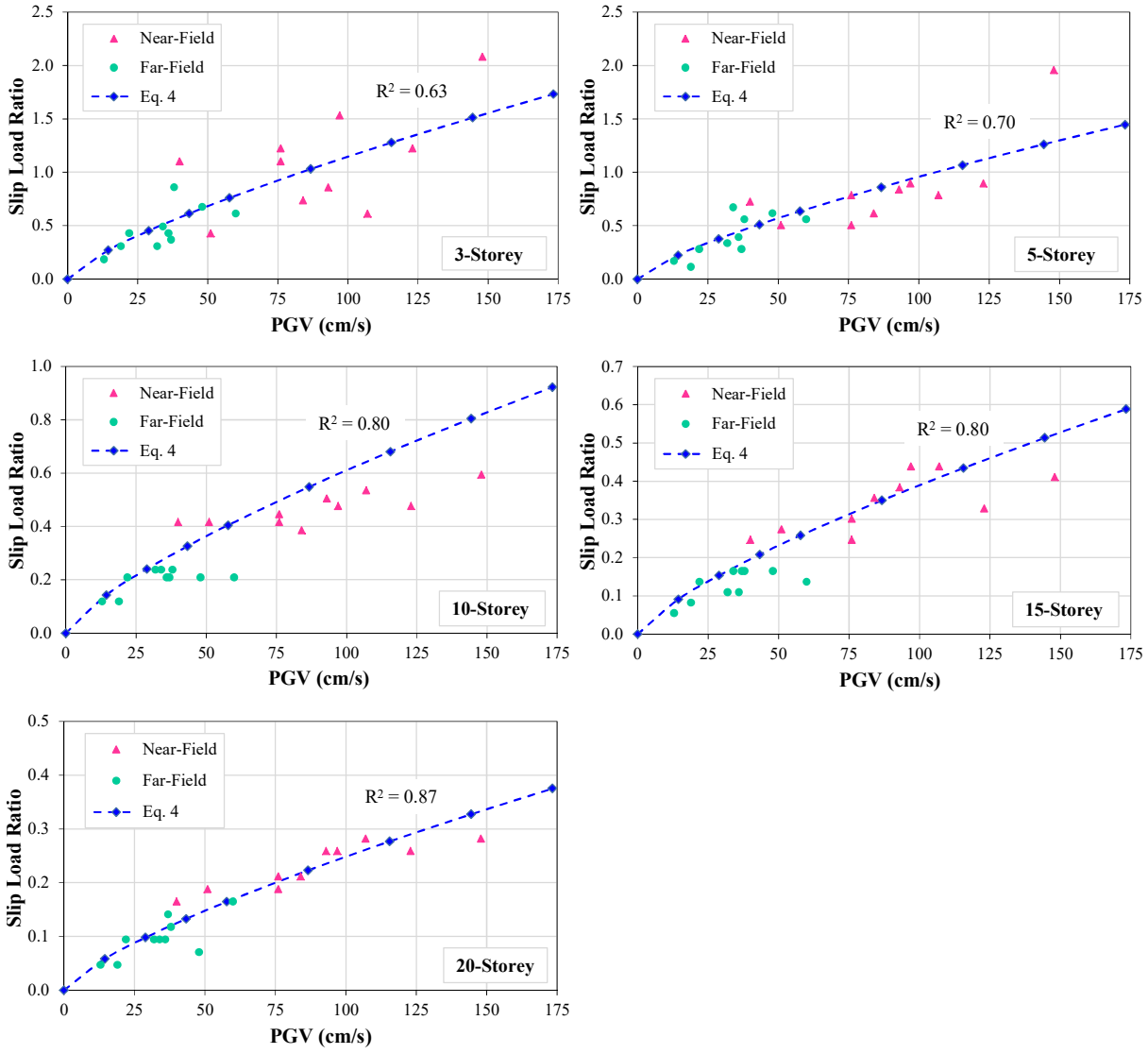

Figure 12. Comparison of optimum slip load ratios for the selected near and far-field earthquakes with the proposed empirical equation (Equation 4) as functions of earthquake PGV level

7. Efficiency of the Proposed Design Method

To assess the efficiency of the proposed design equation, the selected frames were designed using the slip load values obtained from Equation 5 and the following design equation suggested by Nabid et.al [2017]:

$$F_{s,i} = \frac{\sum_{1}^{n} F_{y,i} \times 1.12 \times e^{-0.11n}}{n(n+1)/2} \times (n+1-i) \tag{6}$$

The designed frames were then subjected to the selected near-field and far-field earthquakes. It should be noted that, unlike the equation proposed in this study, Equation (6) does not take into account the characteristics of the design earthquake (i.e. far-field and near-field effects). Figure 13 compares the average ratios between structural responses (i.e. energy dissipation parameters RW and maximum inter-storey drift) obtained by using Equation 5 and Equation 6 for the 3, 5, 10, 15 and 20-storey frames subjected to the selected sets of near and far-field earthquakes. In general, the results indicate that the new design equation (Equation 5) increases the energy dissipation efficiency of the friction devices (i.e. average ratios above 1) and slightly decreases the maximum inter-storey drifts (i.e. average ratios below 1) of the studied frames. Based on the results, on average, the proposed design method could increase the energy dissipation efficiency parameters (RW) of the 3, 5, 10, 15 and 20-storey frames by 17%, 13%, 5%, 21% and 38%, for the selected near-field records and by 62%, 44%, 41%, 54% and 35%, for the far-field earthquakes, respectively. The maximum drift ratios (Equation 5 to Equation 6) are decreased by 20% and 11.4% for the near-field and far-field earthquakes, respectively. While more studies are required to assess the adequacy of the proposed empirical equations for the structures with geometries or structural systems different from those used in this study, the general design methodology proposed in this study should prove useful in preliminary design of friction dampers in practical applications.

It should be mentioned that the proposed friction wall system can be used in combination with the performance-based design methodology proposed by Montuori and Muscati (2016, 2017) to control the failure mechanism in the RC frames. Using this approach allows developing maximum number of dissipative zones at the beam ends, and hence improving the seismic performance of the system under strong earthquakes. The reliability of the design solutions can be also improved by using the partial safety factors related to the resistance model uncertainties in non-linear finite element analyses as proposed by Castaldo et al. (2018).

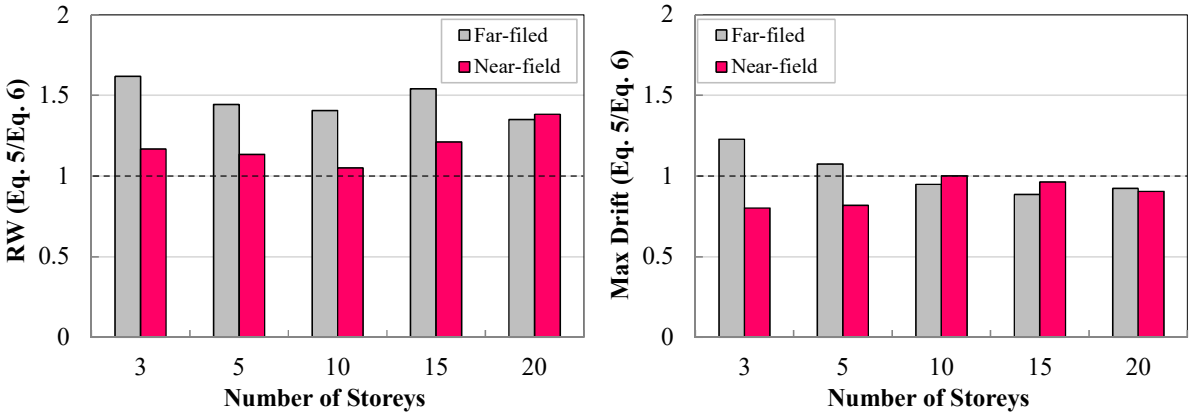

Figure 13. Average ratios (this study to Nabid et al.'s [2017] study) of the (a) energy dissipation parameter (RW) and (b) maximum inter-storey drift for the 3, 5, 10, 15 and 20-storey frames under 20 near and far-field earthquakes

8. Summary and Conclusion

An efficient simplified model was proposed for optimum seismic design of friction-based dampers by considering the effects of near-field and far-field ground motions. To obtain the optimum slip load ranges, a comprehensive parametric study was performed on 3, 5, 10, 15, and 20-storey RC frames with friction wall dampers under spectrum compatible earthquakes scaled to different PGA levels as well as a set of 20 near and far-field earthquake records. Subsequently, empirical equations were proposed to obtain the optimum slip loads based on the number of storeys and PGA (or PGV) of the design earthquake. The efficacy of the proposed design equations in achieving maximum energy dissipation capacity was demonstrated under both near-field and far-field earthquakes. Based on the results of this study, the following conclusions can be drawn:

- Higher PGA (or PGV) levels generally lead to lower energy dissipation efficiency with higher and wider range of optimum slip load ratios. However, the relationship between the PGA and optimum slip load values is not linear and depends on the number of storeys.
- Friction wall dampers exhibit, on average, 118% higher energy dissipation efficiency and 24% lower maximum inter-storey drifts under far-field earthquakes compared to the near-field records. In general, the optimum ranges of slip load ratios obtained for the frames under the near-field earthquakes were also noticeably wider and higher (about 1.5 times) compared to those achieved under the far-field ground motions.
- It was shown that for the same PGV/PGA level (or similar frequency content), the earthquakes with higher PGA and PGV values resulted in higher optimum slip load ratios. In addition, the earthquakes with relatively high velocities occurring at the periods close to the period of the corresponding bare frames result in higher range of optimum slip load values.
- The optimum response of the structures was more sensitive to the variation of PGV than PGA. The proposed design equation for optimum slip load ratio R as a function of PGV resulted in considerably lower dispersions of the results (i.e. higher R-squared values) compared to the equations using PGA as a design variable.
- Compared to the previous equation suggested by Nabid et al. [2017] (without consideration of far-field/ near-field effects), the design method proposed here is considerably more efficient in increasing the energy dissipation efficiency of the friction devices (up to 54%) and decreasing the maximum inter-storey drift of the studied frames (up to 20%).

References

Abrahamson, N. and Somerville, P. [1996] “Effects of the hanging wall and footwall on ground motions recorded during the Northridge earthquake,” Bulletin of the Seismological Society of America 86(1B), S93-S99.

Alavi, B. and Krawinkler, H. [2001] “Effects of near fault ground motions on frame structures,” The John A. Blume Earthquake Engineering Center, Report No. 138, Stanford University, CA.

505 Anderson, J. C. and Bertero, V. V. [1987] "Uncertainties in establishing design earthquakes," Journal of
506 Structural Engineering 113(8), 1709–1724.

507 ASCE/SEI, 41-17, Seismic Rehabilitation of Existing Buildings, 1st edition American Society of Civil
508 Engineers (ASCE), 2017.

509 Bhandari, M., Bharti, S. D., Shrimali, M. K. and Datta, T. K. [2017] "The numerical study of base-isolated
510 buildings under near-field and far-field earthquakes," Journal of Earthquake Engineering 22(6), 989-1007.

511 Bray, J.D. and Rodriguez-Marek, A. [2004] "Characterization of forward-directivity ground motions in the near-
512 fault region," Soil Dynamics and Earthquake Engineering 24(11), 815-828.

513 Castaldo, P. and Tubaldi, E. [2018] "Influence of ground motion characteristics on the optimal single concave
514 sliding bearing properties for base-isolated structures," Soil Dynamics and Earthquake Engineering 104, 346-
515 364.

516 Castaldo, P., Gino, D., Bertagnoli, G. and Mancini, G. [2018] "Partial safety factor for resistance model
517 uncertainties in 2D non-linear finite element analysis of reinforced concrete structures," Engineering Structures
518 176, 746-762.

519 CEN (Comité Européen de Normalization) [2004a]. "Eurocode 8: Design of structures for earthquake
520 resistance-Part 1: General rules, seismic actions and rules for buildings," EN 1998-1-1, Brussels.

521 CEN (Comité Européen de Normalization) [2004b]. "Eurocode 2: Design of concrete structures -Part 1-1:
522 General rules and rules for buildings," EN 1992-1-2, Brussels.

523 Chopra, A.K. and Chintanapakdee, C. [2001] "Comparing response of SDF systems to near-fault and far-fault
524 earthquake motions in the context of spectral regions," Earthquake Engineering and Structural Dynamics,
525 30(12), 1769–1789.

526 Davoodi, M. and Sadjadi, M. [2015] "Assessment of near-field and far-field strong ground motion effects on
527 soil- structure SDOF system," International Journal of Civil Engineering 13, 153-166.

528 Filiatrault, A. and Cherry, S. [1990] "Seismic design spectra for friction-damped structures," Journal of
529 Structural Engineering 116(5), 1334-1355.

530 Guo T. Xu Z. Song L. Wang L. and Zhang Z. [2017]. "Seismic resilience upgrade of RC frame building using
531 self-centering concrete walls with distributed friction devices," Journal of Structural Engineering, ASCE,
532 143(12), 04017160.

533 Hajirasouliha, I. and Doostan, A. [2010] "A simplified model for seismic response prediction of concentrically
534 braced frames," Advances in Engineering Software 41(3), 497-505.

535 Hall, J. F., Heaton, T. H., Halling, M. W. and Wald, D. J. [1995] "Near-source ground motion and its effects on
536 flexible buildings," Earthquake Spectra 11(4), 569-605.

Hatzigeorgiou, G. D. and Pnevmatikos, N. G. [2014] “Maximum damping forces for structures with viscous dampers under near-source earthquakes,” Engineering Structures 68, 1-13.

Housner, G. W. and Jennings, P. C. [1982] “Earthquake design criteria,” EERI Monograph Series, Berkeley, CA.

Iwan, W. D. [1994] “Near-field considerations in specification of seismic design motions for structures,” Proc. of the 10th European Conference on Earthquake Engineering, Vienna, Austria.

Kiris, S. S. and Boduroglu, M. H. [2013] “Earthquake parameters affecting the performance of an RC frame with friction damper,” Soil Dynamics and Earthquake Engineering 55, 148-160.

Lee, S. H., Park, J. H., Lee, S. K. and Min, K. W. [2008] “Allocation and slip load of friction dampers for a seismically excited building structure based on storey shear force distribution,” Engineering Structures, 30, 930-940.

Lin, C. C., Chen, C. L. and Wang, J. F. [2010] “Vibration control of structures with initially accelerated passive tuned mass dampers under near-fault earthquake excitation,” Computer-Aided Civil and Infrastructure Engineering 25(1), 69-75.

Malhotra, P. K. [1999] “Response of buildings to near-field pulse-like ground motions,” Earthquake Engineering and Structural Dynamics 28(11), 1309-1326.

MATLAB [2014]. The MathWorks, Inc.: Natick, Massachusetts, USA.

McKenna, F., Fenves, G. L., Scott, M. H. [2000] “Open system for earthquake engineering simulation,” University of California, Berkeley, California, <http://opensees.berkeley. Edu> (1 August 2016).

Meskouris K., Kratzig W. B. and Hanskotter U. [1992] “Seismic motion damage potential for R/C wall-stiffened buildings In: Fajfar P. and Krawinkler H. (eds) Nonlinear seismic analysis and design of reinforced concrete buildings,” Oxford: Elsevier Applied Science, 125-136.

Miguel, L. F. F., Miguel, L. F. F. and Lopez, R. H. [2016]. “Simultaneous optimization of force and placement of friction dampers under seismic loading,” Engineering Optimization 48, 586-602.

Model Code 2010, The International Federation for Structural Concrete (*fib*), Lausanne, Switzerland, 2012.

Mohammadi, R. K. Mirjalaly, M., Mirtaheri, M., and Nazeryan, M., [2018]. “Comparison between uniform deformation method and Genetic Algorithm for optimizing mechanical properties of dampers,” Earthquakes and Structures 1(14), 1-10.

Montuori, R., Muscati, R. [2016] “A general design procedure for failure mechanism control of reinforced concrete frames,” Engineering Structures 118, 137-155.

Montuori, R., Muscati, R. [2017] “Smart and simple design of seismic resistant reinforced concrete frame,” Composites Part B: Engineering 115, 360-368.

568 Moreschi, L. M., Singh, M. P. [2003]. "Design of yielding metallic and friction dampers for optimal seismic
569 performance." *Earthquake Engineering and Structural Dynamics,* 32, 1291-1311.

570 Mualla I. and Belev B. [2017]. "Overview of recent projects implementing rotational friction dampers," Proc.
571 Of the 13th World Conference on Earthquake Engineering, Santiago, Chile. Paper N° 1667.

572 Nabid, N. [2018] "Performance Based Optimisation of Friction Energy Dissipation Devices in RC Structures",
573 PhD thesis, University of Sheffield, UK.

574 Nabid, N., Hajirasouliha, I. and Petkovski, M. [2017] "A practical method for optimum seismic design of
575 friction wall dampers," Earthquake Spectra 33(3), 1033-1052.

576 Nabid, N., Hajirasouliha, I., and Petkovski, M. [2018] "Performance-based optimisation of RC frames with
577 friction wall dampers using a low-cost optimisation method," Bulletin of Earthquake Engineering 16(10), 5017-
578 5040.

579 Pall, A. S. and Pall, R. T. [2004] "performance-based design using pall friction dampers - an economical design
580 solution," Proc. of the 13th World Conference on Earthquake Engineering, Vancouver, B.C., Canada, Paper No.
581 1955.

582 Papageorgiou, A., Halldorsson, B., and Dong, G. [2002] "TARSCTH (Target Acceleration Spectra Compatible
583 Time Histories)," Engineering Seismology Laboratory (ESL) at the State University of New York at Buffalo.

584 Pasquin, C., Leboeuf, N., Pall, R. T. and Pall, A. [2004] "Friction dampers for seismic rehabilitation of Eaton's
585 building, Montreal," Proc. of the 13th World Conference on Earthquake Engineering, Vancouver, B.C., Canada.

586 Pavel, F. and Lungu, D. [2013] "Correlations between frequency content indicators of strong ground motions
587 and PGV," Journal of Earthquake Engineering 17(4), 543-559.

588 Petkovski, M. and Waldron, P. [2003] "Optimum friction forces for passive control of the seismic response of
589 multi-storey Buildings," Proc. of the 40 years of European Earthquake Engineering SE40EEE. Ohrid,
590 Macedonia.

591 Shiraia k., Kikuchia M., Itob T. and Ishiia K. [2019]. "Earthquake Response Analysis of the Historic Reinforced
592 Concrete Temple Otaniha Hakodate Betsuin after Seismic Retrofitting with Friction Dampers," International
593 Journal Of Architectural Heritage, 13(1), 47-57.

594 Shirkhani, A., Mualla, I. H., Shabakhty, N. and Mousavi, S. R. [2015] "Behavior of steel frames with rotational
595 friction dampers by endurance time method," Journal of Constructional Steel Research, 107, 211–222.

596 Somerville, P. [1998] "Development of an improved representation of near-fault ground motions," SMIP98
597 Seminar on Utilization of Strong-Motion Data, 1-20.

598 Somerville, P. and Smith, N. F. [1996] "Accounting for near-fault rupture directivity effects in the development
599 of design ground motions," Proc. of 11th World Conference on Earthquake Engineering, Acapulco, Mexico,
600 Paper No. 711.

601 Somerville, P. G. [2002] “Characterizing near fault ground motion for the design and evaluation of bridges,”
602 Proc. of the 3rd National Seismic Conference and Workshop on Bridges and Highways, Portland, Oregon, 137-
603 148.

604 Somerville, P., Smith, N. F. and Graves R. W. [1997] “Norman A. Abrahamson; Modification of Empirical
605 Strong Ground Motion Attenuation Relations to Include the Amplitude and Duration Effects of Rupture
606 Directivity,” Seismological Research Letters 68 (1), 199-222.

607 Stewart, J. P. Chiou, S. J., Bray, J. D., Graves, R. W., Somerville, P. G. and Abrahamson, N. A. [2002] “Ground
608 motion evaluation procedures for performance-based design,” Soil Dynamics and Earthquake Engineering
609 22(9), 765-772.

610 Tirca L., Serban O., Tremblay R., Jiang Y. and Chen L. [2018]. “Seismic design, analysis and testing of a
611 friction steel braced frame system for multi-storey buildings in Vancouver,” Key Engineering Materials, 763,
612 1077-1086.

613 Tirca, L. D., Foti, D. and Diaferio, M. [2003] “Response of middle-rise steel frames with and without passive
614 dampers to near-field ground motions,” Engineering Structures 25(2), 169-179.

615 Vezina, S. and Pall, R. T. [2004] “Seismic retrofit of MUCTC building using friction dampers,” Palais des
616 Congres, Montreal. Proc. Of the 13th World Conference on Earthquake Engineering, Vancouver, B.C., Canada,
617 Paper No. 1964.

618 Wald, D. J., Quitoriano, V., Heaton, T. H. and Kanmori H [1999] “Relationships between Peak Ground
619 Acceleration, Peak Ground Velocity, and Modified Mercalli Intensity in California,” Earthquake Spectra 15 (3),
620 555-564.

621 Xu, Z., Agrawal, A. K., He, W. L., and Tan, P. [2007] “Performance of passive energy dissipation systems
622 during near-field ground motion type pulses,” Engineering Structures 29(2), 224-236.

623 Zhu, T. J., Tso, W., and Heidebrecht, A. [1988] “Effect of peak ground A/V ratio on structural damage,” Journal
624 of Structural Engineering 114, 1019-1037.